DEFORMATION MECHANISMS OF TI6AL4V DIAMOND AND OCTET TRUSS LATTICE STRUCTURES PRODUCED THROUGH LASER POWDER BED FUSION (L-PBF)

[1,*]Georgino K. Tshikwand, [2]Deborah C. Blaine, [3]Anton Du Plessis
[1]Department of Mechanical Engineering, Stellenbosch University, South Africa, tshikwadgk@sun.ac.za
[2]Department of Mechanical Engineering, Stellenbosch University, South Africa, dcblaine@sun.ac.za
[3]CT Scanner Facility & Physics department, Stellenbosch University, South Africa, anton2@sun.ac.za

Lattice structures with customized stiffness, strength, and specific strain energy absorption allow for the design of lightweight, loadbearing structures, suitable for functional engineering applications. In this work, we studied the deformation mechanisms of two well-known lattice structure designs produced by laser powder bed fusion (L-PBF) of Ti6Al4V. Two different finite element analysis (FEA) approaches were used to simulate deformation under compression: one using 1D beam elements, the other using 3D solid elements. The results were compared to physical compression tests of L-PBF lattice structures. The octet-truss structure was found to deform by a combination of 45° and 135° shear bands caused by the stretching of the horizontal struts in those planes, whereas the diamond lattice structure was found to deform by 45°shear bands caused by strut bending.

1. INTRODUCTION

Contrary to metal subtractive manufacturing, such as machining where a component is manufactured through the removal of material until the final part is obtained, metal additive manufacturing (AM) is a process of building a component through the fusion of metal powder, layer by layer, until the complete part is produced. As machined parts are usually produced from a wrought blank, there is a high degree of material waste produced as a by-product. AM only uses the material that is needed for the part, and as such has a high level of material economy with low scrap. Additionally, this technology has introduced a new perspective to the manufacturing industry by allowing the designer to build intricate parts for a range of different applications, such as medical, aerospace, automotive. It also shows great potential with biomimetic design approaches [1]. The level of part complexity and ability to build unique or customized shapes, provides significant technical and economic advantages as compared to subtractive manufacturing techniques [2].

Due to the layer-by-layer building process inherent to laser powder-bed fusion (L-PBF), a common AM technique, strut waviness and surface roughness are often introduced, resulting in geometrical differences between the designed structure and the final L-PBF structure [3]. This can influence the mechanical properties of the built structure by affecting the load bearing areas as well as introducing stress concentrations. It thus become challenging to accurately predict the mechanical properties of L-PBF structures, especially those with thin features. Pyka et al. [3] showed how reducing surface roughness features of L-PBF Ti6Al4V lattice structures influenced the mechanical response of these structures. This was attributed to the removal of sharp surface crack initiation sites, which should improve resistance to failure; however, the etching procedure used to remove the rough surface features also reduced the cross-sectional dimensions of the struts, which resulted in reduced strength and stiffness of the structure.

Other influences on the properties of L-PBF produced materials have been studied, such as post-L-PBF heat treatment and its influence on microstructure [4]–[6] and the influence of residual stresses due to the large thermal gradients inherent in the process [7].

Lattice structures are strut-based structures that are built from repeating unit cells in all 3 dimensions throughout the structure. Typically, the struts are thin in comparison to the unit cell volume. A wide range of unit cell designs exist and there are several studies that investigate their design [8]–[11]. For more information on cellular lattice structure design the reader is referred to [1], [12]. Due to the difficulty of machining a lattice structure from a solid blank, AM lends itself as an ideal manufacturing technology for producing these parts. The lattice structure can be built layer-by-layer from a 3D model of the required structure.

[1] The author is enrolled for an M Eng. (Mechanical) degree in the Department of Mechanical and Mechatronics Engineering, Stellenbosch University
*Corresponding author (tshikwadgk@sun.ac.za)

A lattice structure can be considered as a regular porous structure and thus relationships between porosity and properties for porous structures can be used to model their behavior.
Gibson and Ashby [13] conducted extensive studies on naturally occurring irregular porous structures. They proposed the following relationships between the mechanical properties and the relative density, $\left(\frac{\rho}{\rho_s}\right)$, of a porous structure, where ρ is the total material mass per unit volume and ρ_s is the density of the solid material

$$\frac{E}{E_s} = \alpha \left(\frac{\rho}{\rho_s}\right)^n \quad \text{Eq. 1}$$

$$\frac{G}{G_s} = \frac{3}{8}\alpha \left(\frac{\rho}{\rho_s}\right)^n \quad \text{Eq. 2}$$

$$\sigma_{pl} = (0.25 \rightarrow 0.35)\, \sigma_{y,s} \left(\frac{\rho}{\rho_s}\right)^m \quad \text{Eq. 3}$$

Where E and E_s are the Young's modulus of the porous structure and that of the solid material from which the structure is made, respectively. G and G_s are the shear modulus of the porous structure and that of the solid material from which the porous structure is made, respectively. σ_{pl} is the plateau stress and $\sigma_{y,s}$ is the yield stress of the solid material from which the structure is made. n, α and m are constants whose values vary between 1.8 and 2.2, 0.1 and 4, and 1.5 and 2, respectively, depending on the properties and structure (geometry) of the solid material. The plateau stress is the stress at which the porous structure starts to collapse on itself.
Eq. 1, Eq. 2, and Eq. 3 can be used to design a porous, or lattice, structure of prescribed mechanical properties.
The focus of this study was to investigate the mechanical behavior and deformation mechanisms of Ti6Al4V lattice structures subjected to compressive loads. This was determined by simulating the loading condition using finite element methods (FEM) approaches, as well as performing mechanical testing experiments on physical samples. By studying the predicted distribution of different types of stresses induced in the struts during loading and correlating these to the deformation mechanisms observed during mechanical compression testing, the appropriateness of different FEM approaches is evaluated.

2. LATTICE STRUCTURE DESIGN

Lattice structure design for AM requires the determination of lattice structure parameters in order to generate a specific porosity for the lattice, and to ensure the manufacturability of the designed lattice structure. The latter requires a suitable overhang angle and printable dimensions for laser powder bed fusion. Here, the designs are in accordance with the general overhang angle of 45° or higher (45° rule) and within the microscale limits [14].
Lattice structures are often created by repeating unit cell structures in all 3 dimensions.
Analytical equations for the relative density, $\frac{\rho}{\rho_s} = \frac{v}{v_s}$, of a 5 x 5 x 5 lattice structure are derived as a function of the strut thickness. For a specific relative density, a strut thickness is determined. Based on this result, the lattice structure is designed with the help of the CAD software SpaceClaim. This generates a lattice structure with a specific relative density. This relative density is obtained by determine the lattice structure mass properties which is divided by the volume of the solid material, v_s.
We consider the octet-truss and diamond topologies based on the Maxwell criteria that classifies strut-based unit cells as stretch or bending dominated presented here as equation 4 [15].

$$M = m - 3j + 6 \quad \text{Eq. 4}$$

Where m and j are the number of struts and joints respectively.
Eq. 4 is the Maxwell criteria, from which a unit cell is classified as bending-dominated when M is less than 0 and as stretch-dominated when M is approximately 0.
A periodic structure made of stretch or bending dominated unit cells will necessarily be stretch or bending dominated. Figure 1 show the synthesis of the octet-truss and diamond lattice structures' unit cells.

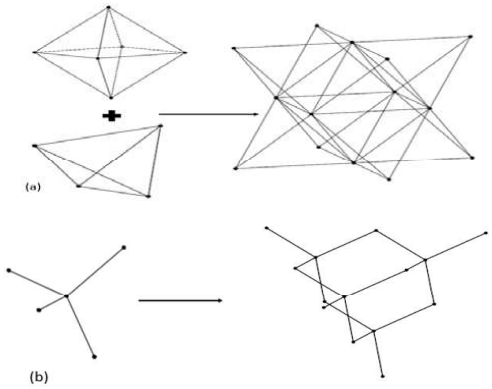

Figure 1 Synthesis of the octet truss (a) and diamond (b) structures

The octet-truss lattice structure is constructed from the combination of the octahedron unit cell with the tetrahedron unit cell at each of the 8 faces of the octahedron unit cell. The octahedron and tetrahedron unit cells both satisfy the condition to be stretch- dominated, thus making the octet truss structure stretch-dominated. The octahedron with 12 struts and 6 joints and the tetrahedron with 6 struts and 4 joints, both unit cells with an M value of 0.

The diamond lattice structure is constructed from 4 diamond unit cells as showns in Figure 1. The diamond unit cell satisfies the condition to be bending-dominated, thus making the whole diamond structure bending-dominated. The diamond with 4 struts and 5 joints, resulting in a negative M value.

For the present study, 5 X 5 X 5 octet-truss and diamond lattice structures were made from the tesselation of the octet-truss and diamond structures of Figure 1, considered here as the building unit cells.

A key concept in the design of lattice structures is the relative density, $\bar{\rho}$, which is the ratio of the density of the lattice structure, ρ_l, to the density of the solid material used to manufacture the lattice structure, ρ_s. The relative density also corresponds to the ratio of the lattice strut volume, v_l, to the total lattice structure volume, v_{tot}.

The determination of the relationship between the relative density and the lattice structure parameters involves the consideration of specific unit cells for each topology, as well as the number of repeating unit cells in the entire lattice structure under review. This is critical as the location of unit cells in the structure, whether the cell is internal or on an outer surface, influences the relative density of the lattice. For this reason, we categorize different types of lattice unit cells according to their position in the lattice, namely

- Core;
- Side;
- Corner or vertex;
- Edge.

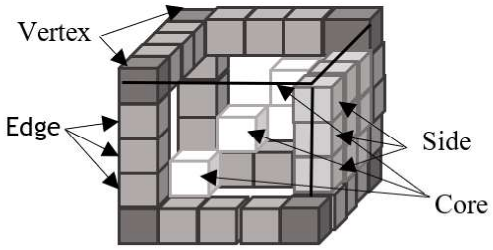

Figure 2 Schematic showing the different types of lattice unit cells, named for their positions in a 5 x 5 x 5 lattice.

Figure 2 indicates the general position and terminology for each cell type in a 5 x 5 x 5 lattice of unit cells. Each block represents a single unit cell, containing the repeating lattice structure within its volume.

5 X 5 X 5 diamond and octet-truss structures contain 3 X 3 X 3 core unit cells and idiosyncratic edge, vertex, and side unit cells. The vertex, edge, and side unit cells contain full cross-section struts located at the outer sides. The full lattice structure was bounded at its upper and lower surfaces by rigid plates.

The volumes of each of the unit cells are added to make $v_l = 27\,\boldsymbol{v_c} + 54\,\boldsymbol{v_s} + 8\,\boldsymbol{v_v} + 36\,\boldsymbol{v_e}$ and the $v_{tot} = 125 * l^3$ is also computed to get the relative density as below,

$$\bar{\rho}_{octet=}\ \frac{1650.03}{125}\sqrt{2}\frac{A}{l^2} \qquad \text{Eq. 5}$$

$$\bar{\rho}_{diamond=}\ \frac{(375+348\sqrt{2})}{125}\frac{A}{l^2} \qquad \text{Eq. 6}$$

Eq. 5 and Eq. 6 are used to calculate the design strut thickness for a fixed relative density. These equations are suitable for beam element design where at the strut joint material is not merged. However, for the solid element design this material is merged and Eq. 5 and Eq. 6 over-estimate the solid lattice volume by about 20 %.

Table 1 shows the geometric parameters for the beam and solid lattice structure design.

Table 1 Geometric parameters of the beam and solid lattice structures

	Beam structure			Solid structure		
	Strut thickness [µm]	Lattice volume [mm^3]	Relative density [%]	Strut thickness [µm]	Lattice volume [mm^3]	Relative density [%]
Diamond-C	423	243.05	24.30	423	201.17	20.12
Diamond-R	375	243.57	24.35	375	201.75	20.18
Octet Truss-C	268	263.25	26.33	268	214.99	21.50
Octet Truss-R	237	262.14	26.21	237	212.08	21.21

Lattice structures are designed with a top and bottom compression platen of 0.200 mm thickness each. This is to allow mechanical compression testing as prescribed in the ISO (13314) standard.

The compression platens add some density to the lattice structure design density. The Ashby Model can be used to scale the mechanical properties of the lattice based on a given relative density. It should also be noted that the nature of strut joints can have an influence on the mechanical properties.

3. FINITE ELEMENT ANALYSIS

Since lattice structures result from the tessellation of unit cells in all 3 dimensions, the first assumption made for the FEM analyses, is to consider an isotropic material model, that is, the material will have the same behavior in all 3 dimensions. This assumption has been proven admissible in many research studies [16]–[19].

Lattice structures consists of a network of struts which experience large deformation when subjected to compressive loads. The determination of mechanical properties and deformation mechanisms from a linear static analysis where only small deformations are considered and the stiffness is independent of the deformation, is appropriate as a first order approximation but will not allow analysis of deformation mechanisms or nonlinear plastic deformation of lattice structures.
Ashby and Gibson recommend determining the elastic modulus from loading the structure into the plastic region to 75% of compressive stress and unloading it [20]. The elastic modulus can be determined from the unloading curve or the linear region curve. Therefore, a nonlinear isotropic material model is appropriate for the FEM simulation of mechanical properties and deformation mechanisms of lattice structures.
Another consideration is the type of nonlinearity to implement in the FEM simulation. There are three types of nonlinearities: material nonlinearity, geometric nonlinearity and contact nonlinearity. Since many lattice structures are not designed with any contact conditions, only material and geometric nonlinearity are considered. Material nonlinearity refers to a material that experience large strain as a result of material plasticity behavior. Geometric nonlinearity refers to the large deformation and change in geometry that a structure can experience when subjected to compressive loading.
The simulation procedure for the nonlinear static analysis will consist of solving a system of nonlinear static equilibrium equations, the details of which are found in [21].
The size of the FEM problem will depend on the discretization method chosen and its shape function or interpolation function. 3D solid and 1D beam elements are commonly used to discretize lattice structure.
Lattice structures are complex structures with many regions that can be regarded as high stress concentration regions, therefore acquiring information in these regions is critical. When the lattice structure is discretized using 3D solid elements, a mesh sensitivity analysis is a common practice to ensure the accuracy of results. A graphical mesh sensitivity analysis was conducted for both topologies as shown in Figure 3. Mesh convergence was achieved between mesh sizes 0.075 mm, 0.100 mm, and 0.150 mm for the diamond lattice structure and 0.100 mm, 0.150 mm, and 0.200 mm for the octet-truss lattice structure. A mesh size of 0.150 mm was selected to reduce the computational time. ANSYS Timoshenko beam elements (BEAM188) were used to mesh the 1D beam element structure and ANSYS 3D solid elements (Solid187) were used to mesh the 3D solid element structure for the purpose FEA compression simulation.

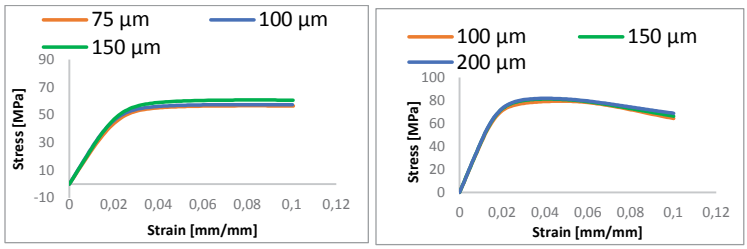

Figure 3 Mesh Convergence analysis of 5 X 5 X 5 3D Solid circular diamond (left) and octet truss (right) lattice structures structure

A FEA compression simulation was conducted following the test method set in ISO (13314) standard for mechanical compression testing of porous metals.
ANSYS academic research Mechanical and CFD (structural/LS-Dyna) was used to conduct the simulation.
Table 2 shows the material properties of Ti6Al4V, of which the yield strength was taken from literature on the mechanical properties of stress relieved SLM Ti6Al4V [22]. the tangent modulus was taken from ANSYS Ti6Al4V material library as shown in Table 2. These material properties were used to define the FEM problem, that is, a nonlinear static analysis. An isotropic hardening was selected to define the plastic region of the material model.

Table 2 ANSYS Ti6Al4V material properties

Temperature (C)	Yield Strength (MPa)	Tangent Modulus (MPa)

20	1098	1332
204	844	1207
427	663	1033
538	527	943
815	60	708
944	21	596

A 1 mm displacement was applied at the top platen in the negative z-direction and the z-translation of the bottom platen was fixed .

Table 3 Material of Ti6Al4V as input for the FEM simulation

Properties	Density [Kg m^{-3}]	Yield Strength [MPa]	Poisson's ratio	Modulus of Elasticity [GPa]	Tangent modulus [MPa]
Value range	4430	1145 [22]	0.3	110	1332

Both the top and bottom plates were modelled as rigid bodies.

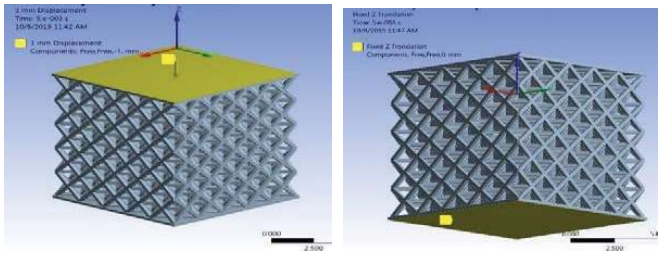

Figure 4 Load and boundary conditions

Table 4 and Table 5show global mechanical properties from the FEA compression simulation results for the beam and solid element cases.

Table 4 1D beam circular and rectangular octet-truss and diamond lattice structures

Topology	Cross section	Young's modulus [GPa]	Yield strength [MPa]	Maximum stress [MPa]	Plateau stress [MPa]
Octet-truss	Rectangular	3.10	72.19	91.99	88.21
	Circular	2.95	67.17	86.87	83.31
Diamond	Rectangular	1.40	33.66	44.60	41.17
	Circular	1.40	31.66	45.10	40.52

Table 5 3D solid circular and rectangular octet-truss and diamond lattice structures

Topology	Cross section	Young's modulus [GPa]	Yield strength [MPa]	Maximum stress [MPa]	Plateau stress [MPa]
Octet-truss	Rectangular	4.32	74.70	93.22	87.92
	Circular	4.20	75.35	92.57	86.60
Diamond	Rectangular	2.38	51.10	65.01	60.38
	Circular	2.46	54.48	68.89	63.80

3.1.1D Beam element result (BEAM188)

Like the determination of the Maxwell criterion result for the diamond structure, the 1D beam simulation results show that this structure is bending-dominated. This is due to the even distribution of reaction bending moments that induce bending stresses across lattice struts. This is seen in Figure 5. A high incidence of uneven distribution of reaction shear and axial forces was also recorded for the diamond structure. The combined effect of the induced normal and shear stresses is given by

the maximum principal stress. This is in Figure 6. The regions of high stress concentration were found to be the strut joints as shown in Figure 5 by the arrows. These high stresses are tensile, the strut fibers stretch at the joint as the strut is bending. These joints are located in a 45° diagonal plane with the horizontal plane. This arrangement causes the formation of shear bands along that plane which can be seen in Figure 5.
A high distribution of reaction axial forces in the struts was observed across struts of the octet-truss lattice structure. These reaction forces induce axial stresses in the struts as seen in Figure 6. Small reaction bending moments and shear forces were observed across some struts of the octet truss structure. A few struts were subjected to high bending stress. This is indicated in Figure 5. The octet truss structure is subjected to higher tensile axial forces in the horizontal struts of the octahedron section and compressive axial forces in the struts of the tetrahedron section as seen in Figure 6. The structure is expected to fail due to the high tensile stress in the horizontal struts.

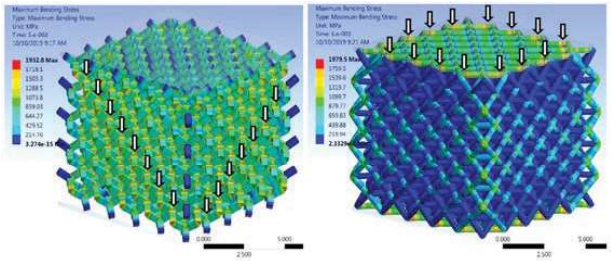

Figure 5 Bending stress distribution in the 1D Beam rectangular diamond (left) and circular octet truss (right) lattice structures

Many FEA software implement either Euler-Bernoulli or Timoshenko beam theories for beam element analysis. Timoshenko beam theory accounts for a constant transverse shear deformation, while Euler-Bernoulli beam theory excludes it. In this case, Timoshenko beam theory is indispensable to capture the shearing behavior of struts. This is found to crucial for the diamond lattice structure because it has thick struts and exhibit extreme bending. It becomes very important to select an appropriate beam theory to obtain the full deformation history of the structure.
Although the beam structure does not fully represent the actual structure in terms of relative density owing to the inability of merging material at strut joints, surface-beam connection, and strut joints, it however provides valuable indications on the deformation behavior of the individual struts in the structure.
From the Beam simulation results, the first signs of deformation are expected at the struts joints and the horizontal struts, for the diamond and octet-truss lattice structure, respectively

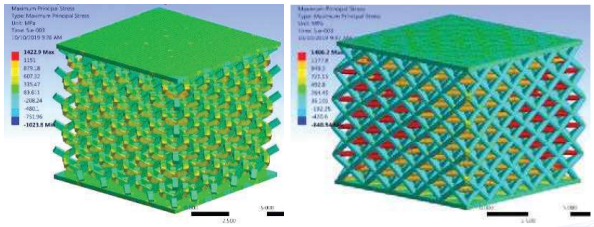

Figure 6 Maximum principal stress distribution in the 1D Beam rectangular struts of the diamond (left) and octet truss lattice (right)

3.2. 3D Solid element result (Solid187)

Like the 1D beam simulation results, the region of high stress concentration for the diamond and octet-truss lattice structures were found to be the strut joints and horizontal struts, respectively. This is indicated in Figure 7 by the arrows.

An eye inspection across the struts in the diamond lattice structure show they are subjected to a high tensile stress at the bottommost side of the strut while the topmost is subjected high compressive stress. This is seen in the opposite order in other struts across the structure based on their location. This arrangement of high tensile and compressive stress at the topmost and bottommost side of the neutral axis of the strut cross-section is an indication of high bending behavior of the strut in question. This bending behavior cause the fibers at the joint to stretch as indicated by the arrows in Figure 7.
This behavior was also observed in the shear stress distribution where in the middle of each strut in the diamond lattice structure, the shear stresses go from positive to negative. This point experiences maximum bending stress. since the shear stress distribution is even, the resulting bending distribution is expected to be even.
For the octet-truss, the struts of the tetrahedral section of the vertex unit cells experience considerable bending as compared to the struts in the other unit cells of the entire structure. The maximum tensile stress is seen in the horizontal struts of the vertex unit cell as indicated by arrows in Figure 7. The other horizontal struts experience tensile stress throughout whereas the struts in the tetrahedron section of the structure are subjected to compressive stresses.

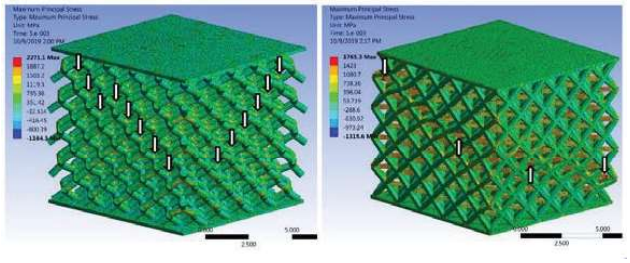

Figure 7 Maximum principal stress distribution of 3D Solid circular diamond (left) and rectangular octet truss (right) lattice structures

This can be also be confirmed by the equivalent plastic strain results seen in Figure 8. it is seen that yielding is mainly localized at the struts' joints and along the horizontal struts in the diamond and octet-truss lattice structures, respectively.
Because the struts' joints are located along 45° plane to the horizontal plane, shear bands are expected about these planes and are the failure modes for diamond structure.
For the octet truss structure, the high plastic strains observed in the horizontal struts cause yielding in the 135° and 45° diagonal planes of the structure. 135° and 45° Shear bands and buckling of struts are expected for the octet-truss lattice structure.

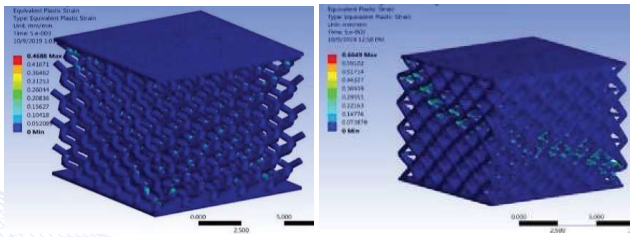

Figure 8 Equivalent Plastic strain distribution of circular diamond (left) and rectangular octet truss (right) lattice structures

4. COMPUTED TOMOGRAPHY (CT) SCAN

The lattice structures were manufactured (selective laser melting) using the M2 Cusing, a concept laser machine, available at the laboratory for advanced manufacturing of Stellenbosch University. The manufacturing process was carried at a laser power of 110 W, a speed of 600 mm/s and a focus diameter of 0.15 mm.

X-ray CT is now increasingly used in additive manufacturing as reviewed in [23]. As outlined in this review paper, besides geometrical measurements, it is also possible to directly simulate CT-scanned geometries using voxel-based simulation. This capability was used to compare different lattice structures previously [24]. The manufactured structures were CT scanned for geometrical analysis using the Phoenix nanotom S, a Nano-CT system available at the CT facility of Stellenbosch University [25]. The scan process was conducted following the guidelines and procedures set out in [25]–[28]. In previous work deformation of micro-lattice structures were also imaged under load using CT, showing in-situ deformation of lattice structures with struts nearing the limit of commercial L-PBF systems [23].

4.1. Geometric parameters

Figure 9 shows the CT images of manufactured structures and the CAD mesh fitted together to show the dimensional deviation.

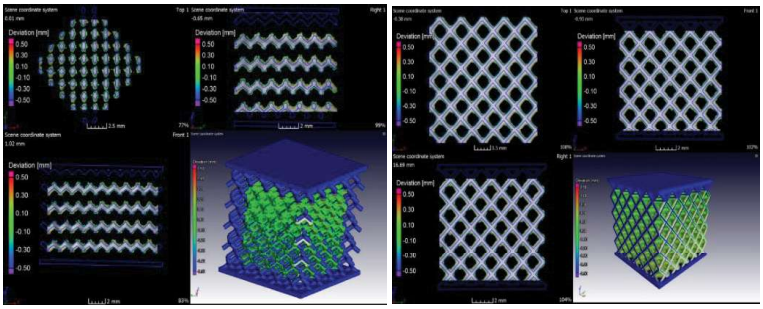

Figure 9 Strut thickness deviation analysis of the CT scan image of the manufactured structures and the 3D CAD mesh for the diamond (left) and octet-truss (right)

The manufactured samples were found to be larger than the 3D mesh used as input for additive manufacturing by a mean deviation margin of 78.9 µm and 65.9 µm across all the struts for the octet-truss and diamond structures respectively. This is an increase in the strut thickness of 29 % and 15.57 % for the octet-truss and diamond lattice structure, respectively. From Eq. 1, Eq. 2, and Eq. 3, it can be shown that the mechanical properties of the manufactured structure will be higher than those of the initial CAD mesh used for their production. For the FEM, approximation of the mechanical behavior of the produced structures, new CAD models were designed based on the new dimensions. The result of these FEM approximations will be compared the mechanical testing results.
After geometrical analysis, no apparent difference was noticeable between the manufactured circular and rectangular cross sections of both topologies.

5. MECHANICAL TESTING

The manufactured structures were heat treated following a stress relief schedule that complies with ASTM standard F2924-14 and SAE H81200D standard (see Table 6).

Table 6 Stress relief heat treatment schedule.

Material	Stress relief temperature	Soaking times
	Degree Celsius	Minutes
Alpha-Beta Alloys		
Ti6Al-4V	650	180

The mechanical compression testing was conducted using the MTS Criterion Model 44, available at the mechanical testing laboratory of Stellenbosch University. Figure 10 shows the experimental set-up for compression testing, where the lower surface is kept stationary and the upper surface is moved by the motion of the crosshead.

The stress relieved samples were compressed uniaxially at a constant crosshead speed of 1 mm/min following the testing method set out in the ISO standard (13314).
The plateau stress, σ_{pl}, was obtained by taking an arithmetic average of stresses at the first peak as shown in **Error! Reference source not found.**. The Young's modulus was calculated by taking 70% and 20% of the plateau stress and corresponding strains.

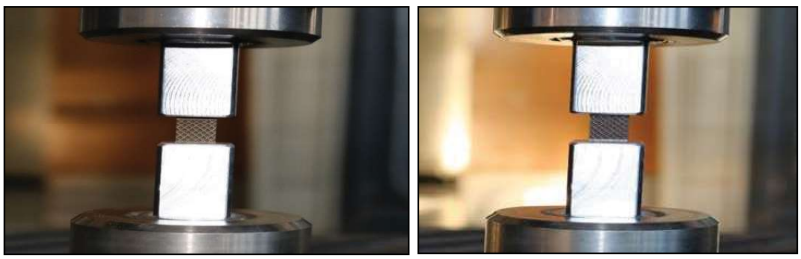

Figure 10 Experimental set-up for compression testing of the octet truss (left) and diamond (right) lattice structures

The Yield strength, σ_y, was considered at 0.2 % strain. This was calculated by first obtaining the zero-strain point. The zero-strain point was found by extending the straight line considered for the calculation of the Young's modulus. A linear equation was obtained, and the zero-strain point determined. This line was then offset 0.002 strain. The yield strength was determined to the intersection of this line and the stress strain curve. This was done for all tested samples and a mean average was obtained.

6. RESULT AND DISCUSSION

Figure 11 shows the stress-strain curves of the octet-truss and diamond lattice structures.
As it can be seen, the first failure in the diamond structure reduces its strength from 120 MPa to 100 MPa (at the next point of failure), whereas the octet truss structure drops from around 180 MPa at its initial failure, to 120 MPa at the next failure. This is indicated by the arrows in Figure 11. The results in Figure 11 are in agreement with previous work on L-PBF diamond-type lattice structures imaged under loading conditions, with the same deformation and fracture modes observed, and the observed experimental elastic modulus lower than those predicted by the models of Ashby, as also found here [29].

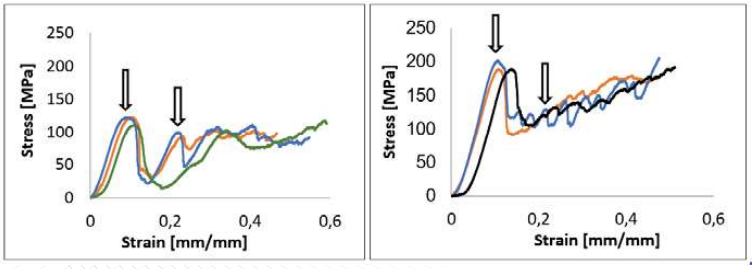

Figure 11 direct stress direct strain results of the experimental mechanical testing for diamond (left) and Octet truss lattice structure (right)

The mechanical properties of both octet-truss and diamond lattice structures are as presented in Table 7 and Table 8, respectively. A comparison between these results and the FEM predicted properties (see Figure 12) is provided.

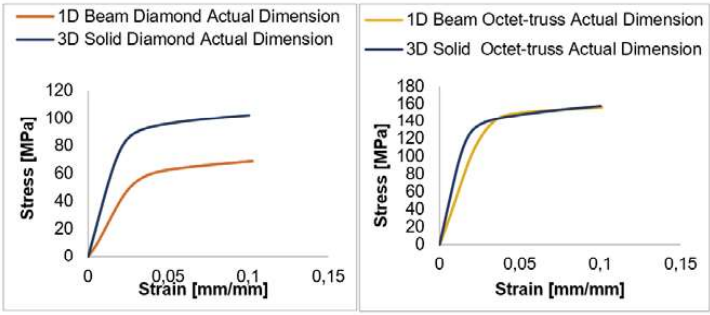

Figure 12 FEM stress-strain curves for 1D Beam and 3D solid diamond (left) and octet-truss lattice structures designed with actual dimensions.

An error of 30 % and below was observed for the yield, maximum and plateau stresses for both the 1D beam and 3D solid octet-truss structure FEM predictions whereas the stiffness was predicted to be 208.33 % more than the actual stiffness.

Table 7 FEM predictions and actual mechanical properties: Octet-truss lattice structure

Octet-truss Lattice structure							
Dimension		cross section	Strut Thickness [µm]	Young's modulus [GPa]	Yield strength [MPa]	Maximum stress [MPa]	Plateau stress [MPa]
Physical Testing				2.4	184.06	196.6	188.97
FEM Actual	3D Solid	circular	347	7.4	128.1	157.61	147.25
% Error				208.33	-30.4	-19.83	-22.08
Physical Testing				2.4	184.06	196.6	188.97
FEM Actual	1D Beam	circular	347	5.1	127.34	156.36	149.6
% Error				112.5	-30.82	-20.47	-20.83

For the diamond structure, only the 3D solid FEM predicted the yield, plateau and maximum stresses within less than 25 % error whereas the 1D beam FEM predicted within larger errors as seen in Table 8.

Table 8 FEM predictions and actual mechanical properties: Diamond lattice structure

Diamond Lattice structure							
Dimension		Cross-section	Strut Thickness [µm]	Young's modulus [GPa]	Yield strength [MPa]	Maximum stress [MPa]	Plateau stress [MPa]
Physical Testing			489	1.8	107.1	121.11	117.49
FEM Actual	3D Solid	circular		4.43	81.21	102.44	95.91
% Error				146.11	-24.17	-15.42	-18.37
Physical Testing			489	1.8	107.1	121.11	117.49
FEM Actual	1D Beam	circular		2.1	49.56	80.46	62.21
% Error				16.67	-53.73	-33.56	-47.05

Figure **13** shows the predicted deformation mechanisms obtained through the equivalent plastic strain. This pattern of the equivalent plastic strain was obtained by conducting a large strain, large displacement FEM analysis. This analysis only provides plastic strain results of struts whose geometry

has been considerably changed by the applied load. The strut regions are those where yielding is likely to take place.

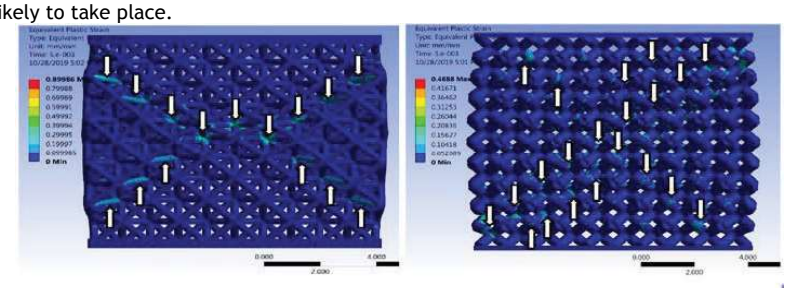

Figure 13 FEM predicted deformation pattern for the octet-truss (left) and diamond lattice structure

High plastic strains are observed in the horizontal struts of the octahedral section of unit cells located in 45° and 135° diagonal planes. This is seen and indicated by arrows in Figure **13** (left). Figure 6 and Figure 7 show how the horizontal struts were subjected to high tensile stresses during compression of the entire structure. This deformation mechanism was observed in the experimental results (see Figure 14) which show identical deformation pattern. This can be seen that once full compression of the octet-truss structure is reached, as in the last two pictures of Figure 14.
High plastic strains are seen at strut joints in the diamond lattice structure as seen in Figure **13** (right). This correlates to the region of high stress concentration seen in Figure 6 and Figure 7. In these figures, it is seen that as the structure is compressed, the strut bend outward from the strut joints. This causes fibers at the joint to stretch. The entire structure experienced failure along 45° diagonal planes, as shown in Figure 7. This forms shear band type of failure. Figure 15 show the produced diamond structure. It is seen that as failure progresses, parallel diagonal planes collapse onto each other. A better picture of the shear band can be seen in the fourth picture in Figure 15, where full compression of the structure was reached.

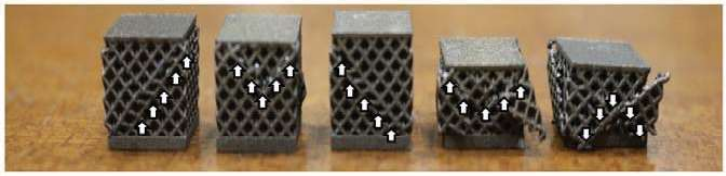

Figure 14 Compressed octet truss sample

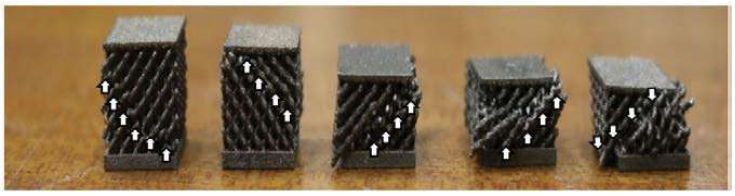

Figure 15 Compressed diamond sample

Figure 16 shows crack propagation at the strut joints of the diamond structure hereby confirming the 3D Solid FEM prediction. The 3D FEM predicted that failure would initiat at the strut joints.

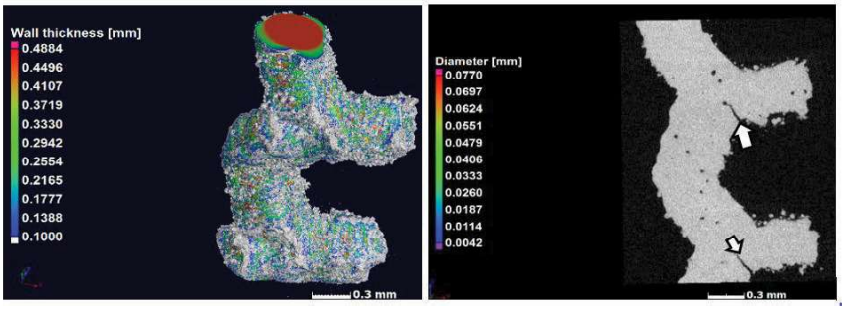

Figure 16 CT Scan of a series of struts showing the crack propagation at the strut joints.

CONCLUSION

The investigation of the mechanical behavior and the deformation mechanisms of the octet truss and diamond lattice structures was the main objective of the present study. Octet-truss and diamond lattice structures of fixed porosity and structure thickness were selected. They were designed using an iterative process of calculating the strut volume as a function of thickness until the desired structure was obtained. Design equations for the relative density were derived based on this process. FEA compression simulation were conducted on the 1D beam and 3D solid mesh using ANSYS academic research Mechanical and CFD (structural/LS-Dyna). Preliminary results show that a FEM analysis could predict the compressive properties of the selected lattice structure with limits. A large strain only FEM analysis was enough to predict the mechanical properties of structure whereas a large strain, large displacement FEM analysis predicted the deformation mechanisms of the selected structures. No fracture or damage model was used to visualize the failure initiation in the FEM results. However, the selected material properties and plasticity model gave ample information about the stress and strain distribution which were used to predict the deformation mechanisms of the structures. These agreed with the deformation mechanisms of the mechanical testing results.
Following are the observed deformation mechanisms of both octet-truss and diamond structures as predicted by FEA and confirmed by mechanical testing:

- The diamond lattice structures were found to be bending-dominated, as is evidenced by the high reaction bending stresses (see Figure 5) evenly distributed across all struts, and shear and axial stresses distribution. High bending occurs in the middle of the strut where a transition from positive to negative shear indicates maximum bending moment. The bending moments induce high bending stress at the strut joints. This causes the structure to fail about these joints, forming 45° shear bands. Parallel diagonal planes collapse onto each other as the structure is fully compressed (see Figure 15).
- The octet-truss lattice structures were found to be stretch-dominated, as is evidenced by high axial stresses in the struts (see Figure 6 and Figure 7). The plastic strain distribution across the structure places the region of high plastic strain (high stress concentration) along the length of the horizontal struts located in diagonal or cross-diagonal planes on the four faces of the structure. High 45° and 135° shear bands along these planes were predicted by the plastic strain distribution. This is confirmed by the mechanical testing.
- Mechanical testing confirmed the predicted deformation mechanisms of both structures. 45° shear band failure for the diamond lattice structure, and 45° and 135° shear bands failure for the octet-truss lattice structure. High compressive buckling of struts was observed at the interface of the bottom platen.(see Figure **13**, Figure 14 and Figure 15)

ACKNOWLEDGEMENT

The funding for this project came from the collaborative program for additive manufacturing (CPAM, NRF) whom we thank dearly. The main author acknowledges Prof Anton Du Plessis and Prof. Deborah Blaine for their supervision throughout the course of this project.

REFERENCES

[1] A. du Plessis *et al.*, "Beautiful and Functional: A Review of Biomimetic Design in Additive

Manufacturing," *Addit. Manuf.*, vol. 27, no. March, pp. 408–427, 2019.
[2] "Bridging the gap with 3D printing." [Online]. Available: https://www.airbus.com/newsroom/news/en/2018/04/bridging-the-gap-with-3d-printing.html. [Accessed: 02-Jul-2018].
[3] A. Burakowski *et al.*, "Surface Modification of Ti6Al4V Open Porous Structures Produced by Additive Manufacturing," *Adv. Eng. Mater.*, vol. 14, no. 6, pp. 363–370, 2012.
[4] B. Vrancken, L. Thijs, J. Kruth, and J. Van Humbeeck, "Heat treatment of Ti6Al4V produced by Selective Laser Melting□: Microstructure and mechanical properties," *J. Alloys Compd.*, vol. 541, pp. 177–185, 2012.
[5] L. Thijs, F. Verhaeghe, T. Craeghs, J. Van Humbeeck, and J. P. Kruth, "A study of the microstructural evolution during selective laser melting of Ti-6Al-4V," *Acta Mater.*, vol. 58, no. 9, pp. 3303–3312, 2010.
[6] L. E. Murr *et al.*, "Microstructure and mechanical behavior of Ti-6Al-4V produced by rapid-layer manufacturing, for biomedical applications," *J. Mech. Behav. Biomed. Mater.*, vol. 2, no. 1, pp. 20–32, 2009.
[7] P. Mercelis, J. P. Kruth, P. Mercelis, and J. Kruth, "Residual stresses in selective laser sintering and selective laser melting," 2012.
[8] I. Maskery *et al.*, "Insights into the mechanical properties of several triply periodic minimal surface lattice structures made by polymer additive manufacturing," *Polymer (Guildf).*, vol. 152, pp. 62–71, 2018.
[9] S. R. Johnston, D. W. Rosen, M. Reed, and H. V. Wang, "Analysis of Mesostructure Unit Cells Comprised of Octet-truss Structures," pp. 421–432, 2006.
[10] L. E. Murr *et al.*, "Next-generation biomedical implants using additive manufacturing of complex cellular and functional mesh arrays," *Philos. Trans. R. Soc. A Math. Phys. Eng. Sci.*, vol. 368, no. 1917, pp. 1999–2032, 2010.
[11] A. du Plessis, I. Yadroitsava, and I. Yadroitsev, "Ti6Al4V lightweight lattice structures manufactured by laser powder bed fusion for load-bearing applications," *Opt. Laser Technol.*, vol. 108, pp. 521–528, 2018.
[12] D. Bhate, C. Penick, L. Ferry, and C. Lee, "Classification and Selection of Cellular Materials in Mechanical Design: Engineering and Biomimetic Approaches," *Designs*, vol. 3, no. 1, p. 19, 2019.
[13] L. J. Gibson and M. F. Ashby, *Cellular solids□: structure and properties*. Cambridge University Press, 1999.
[14] L. Hirt, A. Reiser, R. Spolenak, and T. Zambelli, "Additive Manufacturing of Metal Structures at the Micrometer Scale," *Adv. Mater.*, vol. 29, no. 17, 2017.
[15] J. C. Maxwell, "L. *On the calculation of the equilibrium and stiffness of frames*," *London, Edinburgh, Dublin Philos. Mag. J. Sci.*, vol. 27, no. 182, pp. 294–299, Apr. 1864.
[16] T. Tancogne-Dejean, A. B. Spierings, and D. Mohr, "Additively-manufactured metallic micro-lattice materials for high specific energy absorption under static and dynamic loading," *Acta Mater.*, vol. 116, pp. 14–28, 2016.
[17] M. Helou, S. Vongbunyong, and S. Kara, "Finite Element Analysis and Validation of Cellular Structures," *Procedia CIRP*, vol. 50, pp. 94–99, 2016.
[18] M. Helou and S. Kara, "Design, analysis and manufacturing of lattice structures: An overview," *Int. J. Comput. Integr. Manuf.*, vol. 31, no. 3, pp. 243–261, 2018.
[19] R. Hedayati, M. Sadighi, M. Mohammadi-Aghdam, and A. A. Zadpoor, "Mechanical properties of regular porous biomaterials made from truncated cube repeating unit cells: Analytical solutions and computational models," *Mater. Sci. Eng. C*, vol. 60, pp. 163–183, 2016.
[20] J. W. H. and H. N. G. W. M.F. Ashby, A.G. Evans, N.A. Fleck, L.J. Gibson, "Metal Foams□: A Design Guide Metal Foams□: A Design Guide."
[21] K.-J. Bathe, *Finite Elment Procedures*. 2016.
[22] V. Cain, L. Thijs, J. Van Humbeeck, B. Van Hooreweder, and R. Knutsen, "Crack propagation and fracture toughness of Ti6Al4V alloy produced by selective laser melting," *Addit. Manuf.*, vol. 5, pp. 68–76, 2015.
[23] A. Du Plessis, D.-P. Kouprianoff, I. Yadroitsava, and I. Yadroitsev, "materials Mechanical Properties and In Situ Deformation Imaging of Microlattices Manufactured by Laser Based Powder Bed Fusion," 2018.
[24] A. du Plessis, I. Yadroitsev, I. Yadroitsava, and S. G. Le Roux, "X-Ray Microcomputed Tomography in Additive Manufacturing: A Review of the Current Technology and

Applications," *3D Print. Addit. Manuf.*, vol. 5, no. 3, pp. 227–247, 2018.
[25] A. Plessis and S. G. Roux, "X-RAY MICRO-CT SUPPORTING THE SOUTH AFRICAN ADDITIVE MANUFACTURING COMMUNITY A. du Plessis 1* , S.G. le Roux 2," no. November, 2018.
[26] A. du Plessis, I. Yadroitsava, I. Yadroitsev, S. G. le Roux, and D. C. Blaine, "Numerical comparison of lattice unit cell designs for medical implants by additive manufacturing," *Virtual Phys. Prototyp.*, vol. 13, no. 4, pp. 266–281, 2018.
[27] A. Plessis, S. G. Roux, and M. Tshibalanganda, "Advancing X-ray micro computed tomography in Africa : Going far , together," vol. 3, 2019.
[28] A. du Plessis, C. Broeckhoven, A. Guelpa, and S. G. le Roux, "Laboratory x-ray micro-computed tomography: a user guideline for biological samples," *Gigascience*, vol. 6, no. 6, pp. 1–11, Jun. 2017.
[29] A. Du Plessis, D.-P. Kouprianoff, I. Yadroitsava, and I. Yadroitsev, "Mechanical Properties and In Situ Deformation Imaging of Microlattices Manufactured by Laser Based Powder Bed Fusion," *Materials (Basel).*, vol. 11, no. 9, p. 1663, 2018.